PAPER NAME
yer-2201-15 (1).pdf

AUTHOR
Ahmad Zaenudin

WORD COUNT
12083 Words

CHARACTER COUNT
54857 Characters

PAGE COUNT
14 Pages

FILE SIZE
4.2MB

SUBMISSION DATE
Aug 14, 2022 12:59 PM GMT+7

REPORT DATE
Aug 14, 2022 1:02 PM GMT+7

13% Overall Similarity

The combined total of all matches, including overlapping sources, for each database.

- 9% Internet database
- 9% Publications database
- Crossref database
- Crossref Posted Content database
- 8% Submitted Works database

Excluded from Similarity Report

- Bibliographic material
- Cited material

TÜBİTAK

Turkish Journal of Earth Sciences

http://journals.tubitak.gov.tr/earth/

Research Article

Turkish J Earth Sci
(2022) 31:

doi:10.55730/yer-2201-15

Shear wave velocity estimation based on the particle swarm optimization method of HVSR curve inversion in Bakauheni district, Indonesia

Ahmad ZAENUDIN[1], I Gede Boy DARMAWAN[1], Alhada FARDUWIN[2], Rahmat Catur WIBOWO[1,*]

[1]Department of Geophysical Engineering, Faculty of Engineering, University of Lampung, Bandar Lampung, Indonesia

[2]Department of Geophysical Engineering, Faculty of Production and Industrial Technology, Institute of Sumatera Technology, South Lampung, Indonesia

Received: 26.01.2022 • **Accepted/Published Online:** 21.06.2022 • **Final Version:** 00.00.2022

Abstract: The Nakamura method, known as horizontal to vertical spectral ratio (HVSR), has been used to analyze site effect assessment. Over the past decade, various HVSR curve inversion methods for near-surface geophysical surveys have been developed. Particle swarm optimization (PSO) inversion method has been applied to solve the HVSR inversion curve to estimate the shear wave velocity (V_s) value towards the depth. In this study, the HVSR curve inversion experiment has been applied with two synthetic data, noise-free data and the other is contaminated by 10% random noise. This research aims to find out how the PSO algorithm performs to find the best solution. The result indicated that the PSO algorithm is relatively stable fast in converging and producing the solution closely with the actual model. Finally, we obtained a fit model on actual data inversion that shows the V_s value towards depth from PSO inversion and is able to describe the fault model and sediment layer in Way Baka fault.

Key words: HVSR, PSO, shear wave velocity, Way Baka fault

1. Introduction

Since the 1990s, the HVSR method has become a popular method for investigating shallow subsurface structures. This method was first introduced by Nogoshi and Igarashi (1970, 1971) and massively developed by Nakamura (1989, 2000), commonly known as the Nakamura method. This method utilizes ambient seismic noise (microtremor) signals recorded in three seismograph components (NS, EW, and V). HVSR or H/V value was obtained by calculating the ratio between horizontal (NS and EW) and vertical components (frequency domain). The dominant frequency (f_0) and peak amplitude (amplification) values can be obtained from those ratio values, and those values will be used to analyze the subsurface geological condition.

Guéguen et al. (2007) state that the HVSR method is commonly used for three scientific purposes an f_0, various resonance, and sediment layer evaluation. The HVSR method applications cover the various scientific field, including geology (Mantovani et al., 2017), seismology, micro zonation study (Scherbaum et al., 2003; Gallipoli et al., 2004; D'Amico et al., 2008; Paolucci et al., 2015), engineering (Mucciarelli and Gallipoli, 2001; Gallipoli et al., 2018;), soil and fault investigation (Harutoonian et al., 2013; Akkaya, 2015; Setiawan et al., 2018; Akkaya and Özvan, 2019; Khalili and Mirzakurdeh, 2019), and even in archeology (Wilken et al., 2015; Zeid et al., 2016; Bignardi et al., 2017; Zeid et al., 2017a, 2017b).

The HVSR processing stage is intended to obtain horizontal and vertical ratio curves at a specific site in the measurement location. The three recorded seismic components will be divided by the desired window length into several windows. Each window is then performed Fourier transform for all parts, curves smoothing, and ratio calculation between the horizontal and vertical components. The number of generated curves will be comparable with the number of windows. The average value will be calculated from all the curves to obtain the HVSR curve as a frequency function. The HVSR curve consists of peaks that describe the subsurface layer above the bedrock layer. Generally, if there is more than one peak amplitude in the HVSR curve, the peak with the lowest frequency is called resonant (f_0).

Nakamura (1989) stated that HVSR peak amplitude results from multiple reflections of body waves. However, in 2000, Nakamura developed a theory stating that a combination of surface wave and body wave affects the shape of the HVSR curve. It depends on the visco-elastic parameter of the layer, distance, and source distribution

* Correspondence: rahmat.caturwibowo@eng.unila.ac.id

(Bonnefoy-Claudet et al., 2006). The HVSR curve will show local maximum on S-wave resonance frequency regardless of that wavefield nature.

HVSR is used in two stages. The first stage involves data processing to determine an f_0. In the final stage, the HVSR curve can be inverted to obtain the subsurface layer by viscoelastic parameter value (Tsai and Housner, 1970; Aki and Richards, 2002; Lunedei and Albarello, 2010; Sánchez-Sesma et al., 2011; Lunedei and Malischewsky, 2015). This inversion process will provide the velocity model of the subsurface layer that will be useful for the seismic section comparison and application in other engineering fields. Some scientists have developed various tools and inversion methods. For example, Herak (2008) developed the HVSR model through inversion with a Monte Carlo-based algorithm. Likewise, in processing 2D and 3D HVSR models, inversion with a Monte Carlo-based algorithm is used in the OpenHVSR software (Bignardi et al., 2016; Bignardi et al., 2017; Bignardi et al., 2018). At the same time, García-Jerez et al. (2016) performed an inversion based on the simulated annealing (SA) and interior point (IP) algorithms.

The HVSR curve inversion was done in this study to obtain the V_s towards depth using the PSO algorithm. This algorithm has been used to optimize and solve inversion problems in various engineering fields, such as electronic, electromagnetic, expert systems, machine learning, network, scheduling, energy, metallurgy, biomedical engineering, and finance. In geophysics, this method also succeeded in vertical electrical sounding data inversion (Fernández-Martínez et al., 2010), Rayleigh wave inversion (Sungkono and Santosa, 2011; Laby et al., 2016), magnetic (Essa and Elhussein, 2020), gravity (Pallero et al., 2017) and electromagnetic inversion (Godio and Santilano, 2018; Pace et al., 2019). Ding et al. (2019) did a study to compare accuracy and efficiency between PSO and GA (Genetic Algorithm) to determine the kinetic parameters of the biomass pyrolysis reaction and show a result that PSO is faster towards convergent and has a closer solution to the global optimum. Göktürkler and Balkaya (2012) did the inversion of SP anomalies caused by simple-geometry bodies using three metaheuristics including PSO, GA, and SA, and show that PSO is faster than GA and SA. Ekinci et al. (2019) presented the results of parameter estimations of gravity and magnetic anomalies due to deep-seated faults using PSO and DE. The result shows that DE is superior to PSO in the case of geophysical potential field methods.

2. Method of experimental study

The HVSR method is based on ambient noise measurement on a specific site. Ambient noise, usually called microtremor, appears anywhere on the earth's surface related to atmospheric phenomena and anthropogenic activity (Gutenberg, 1936; Asten, 1978). Microtremor is often characterized by minimal wave oscillation (10^{-4} to 10^{-2} mm) with a spectral component that is significantly attenuated and can be measured with a passive recording method. The elastic wave propagation from a source to receiver experiences an attenuation usually caused by a geometric factor (wavefront dimension escalation) and inelastic (intrinsic). However, not all rocks are perfectly elastic, especially sediment (Sarkowi et al., 2022).

$$HVSR = \frac{H(f)}{V(f)} \tag{1}$$

$$H(f) = \sqrt{E(f)^2 + N(f)^2} \tag{2}$$

where $H(f)$ is the amplitude spectral of horizontal component, $V(f)$ is the amplitude spectral of vertical component, $E(f)$ is the amplitude spectral of EW component, and $N(f)$ is the amplitude spectral of the NS component. The spectral ratio between horizontal and vertical components of ambient noise shows peak value on a specific frequency that is related with f_0 of ground layer thickness (Seht and Wohlenberg, 1999):

$$h = af_o^b \tag{3}$$

where h is the depth of sediment layer (Quaternary), a and b are correlation coefficients related to geometry and geotechnical properties in the site. HVSR data is controlled by impedance contrast in each depth, where a high-velocity difference will result in the HVSR curve with a sharp peak resonance value. In some cases, a comparison between HVSR and other geophysical data (downhole profile, MASW profile, gravity anomaly) shows that a high and sharp HVSR curve peak value resulted from a high sediment or basement layer with velocity contrast value. In other cases, effects like these are also associated with a thin sediment layer (Maresca et al., 2018).

3. Theory of PSO algorithm

In geophysics, two types of modeling are commonly used: forward and inverse modeling. Forward modeling states the data calculation process theoretically observed on the earth's surface if the subsurface model parameter value is known. That theoretical data calculation uses a mathematical equation derived from physics concepts underlying the phenomenon under review. A fit model can be obtained using the trial-and-error method of model parameters in forwarding modeling so that the resulting model can represent the actual subsurface conditions. Meanwhile, inversion modeling is the opposite of forwarding modeling, in which model parameter is derived directly from field data.

Inversion theory is defined as a mathematics and statistic method to obtain information about a physics

system based on observation of that system. The physics system in question is a reviewed phenomenon. The observation result of the system is data. Meanwhile, information that will be obtained from data is a model or model parameter. Suitability between model response and observation data is stated by an objective function (misfit) that should be minimized. The searching process of that minimum objective function is associated with the optimum model's searching process, which minimum characteristic of that function is used for model parameter searching. Then inversion modeling only can be performed if the forward modeling function is known. To obtain an optimum solution, then that function should be optimized. A local and global approach can achieve that optimization. The local approach is trapped easily in a local minimum, and the final solution depends on the given initial model parameter. The global approach will find solutions in the global minimum and does not need an initial model parameter but needs a model predetermined search space that has been decided. One of the global optimization methods in geophysical inversion is particle swarm optimization (PSO).

PSO is a computational technique that adapted the social behavior of a flock of birds (particles) to find food (Kennedy and Eberhart, 1995). Each behavior in searching for food or a target is influenced by individual intelligence and collective behavior. When an individual finds the shortest way to their target, other individuals in a group will follow that quickest way. Everyone has information related to location and speed towards each target expressed in vectors $\boldsymbol{X}$ and V. Everyone submits that information to other individuals and then adjusts their speed (V) and position ($\boldsymbol{X}$) based on the received data. The objective function is a target of the individual swarm that will be optimized. The purpose is to obtain vector $\boldsymbol{X}$ while the objective function is in the global optimum. In an inversion, vector $\boldsymbol{X}$ contains model parameter (m) that is estimated on HVSR curve inversion. In this case, the model parameter is layer thickness (H) and the velocity of shear waves (V_s).

PSO algorithm steps are as follows:

a. Early initiation determines the number of particles and iterations that will be used in optimization. In this step, the search space model also decided to find the value of $\boldsymbol{X}$ ($\boldsymbol{X}_{min} \leq \boldsymbol{X} \geq \boldsymbol{X}_{max}$), in which $\boldsymbol{X}$ is posterior that contains a set of inversion solutions.

b. $\boldsymbol{X}$ initial population generated from random search space, so the initial population is obtained $\boldsymbol{X}_1^0, \boldsymbol{X}_2^0, \boldsymbol{X}_3^0, \ldots, \boldsymbol{X}_j^i$; *i = iteration*; *j = n – th particle*; *n = number of particle*.

For initial iteration of V value set to zero ($V_1^0 = V_2^0 = V_3^0 = \cdots = V_i^0 = 0$.)

c. Objective function evaluation from each particle that is raised so an objective function value is obtained $f[\boldsymbol{X}_1^0]; f[\boldsymbol{X}_2^0]; f[\boldsymbol{X}_3^0; \ldots.; f[\boldsymbol{X}_j^0]$.

d. Determination of the parameter of l and g; l is the best position for each particle in the given iteration. Meanwhile, g is the best position that the particle can reach in a group. The best indicator is seen from its objective function value, which is the best place when the f value is minimum.

e. Update the V and $\boldsymbol{X}$ values using the PSO algorithm (eq. 1) for each iteration. V and $\boldsymbol{X}$ values are calculated with the following equation:

$$\begin{aligned} v_i(k+1) &= \omega v_i(k) + \phi_1\big(g(k) - x_i(k)\big) + \phi_2\big(l_i(k) - x_i(k)\big) \\ x_i(k+1) &= x_i(k) + v_i(k+1) \end{aligned} \tag{4}$$

where

$$\phi_1 = r_1 a_g, \qquad \phi_2 = r_2 a_l, \qquad r_1, r_2 \longrightarrow U(0,1)\ \omega, a_l, a_g \in \mathbb{R} \tag{5}$$

$l_i(k)$ is the best position of the *i-th* particle, $g(k)$ is the best global position, ω is inertia moment, ϕ_1 and ϕ_2 are global and local acceleration, and α_l, α_g are global and local acceleration constants.

By applying regressive discretization (RR-PSO) on velocity and acceleration in time function (Fernández-Martínez and GarcÍa-Gonzalo, 2012), obtained a discrete model with the equation as follows:

$$\begin{aligned} x'(t) &\simeq \frac{x(t) - x(t-\Delta t)}{\Delta t} \\ x''(t) &\simeq \frac{x(t) - 2x(t-\Delta t) + x(t-2\Delta t)}{\Delta t^2} = \frac{x'(t) - x'(t-\Delta t)}{\Delta t} \end{aligned} \tag{6}$$

By applying the following equations relation,

$$x(t) = (x(t-\Delta t) + v(t)\Delta t$$

$$\frac{v(t) - v(t-\Delta t)}{\Delta t} + (1-\omega)v(t) + \phi(x(t-\Delta t) + v(t)\Delta t) = \phi_1 g(t-t_0) + \phi_2 l(t-t_0)$$

,

$$v(t) = \frac{v(t-\Delta t) + \phi_1 \Delta t\big(g(t-t_0) - x(t-\Delta t)\big)}{1 + (1-\omega)\Delta t + \phi\Delta t^2} + \frac{\phi_2 \Delta t\big(l(t-t_0) - x(t-\Delta t)\big)}{1 + (1-\omega)\Delta t + \phi\Delta t^2} \tag{7}$$

Then the equation for RR-PSO mathematically can be written as follows:

$$v(t-\Delta t) = \frac{v(t) + \phi_1 \Delta t\big(g(t) - x(t)\big) + \phi_2 \Delta t\big(l(t) - x(t)\big)}{1 + (1-\omega)\Delta t + \phi\Delta t^2}$$

$$x(t+\Delta t) = x(t) + v(t+\Delta t)\Delta t;\ \ t, \Delta t\, \epsilon \mathbb{R}$$

$$x(0) = x_0;\ v(0) = v_0;\ \phi = \phi_1 + \phi_2 \tag{8}$$

In PSO terminology, the searched geophysical model is called a particle. Each particle has position and velocity information in the model search space. PSO algorithm will update position $x_i(k)$ and velocity $v_i(k)$ for each particle in the swarm. The velocity of each i-particle in every k-iteration is influenced by inertia moment (ω), social intelligence, and cognitive intelligence.

3.1. PSO inversion scheme to inverse HVSR curve

The tuning parameter value is significant in performing PSO inversion to obtain the best result. The tuning

parameter value that we use refers to (Fernández-Martínez et al., 2010) with $\omega = 0.8$; $a_l = 1.8$ and $a_g = 2$. This tuning parameter was used by Laby et al. (2016) and Farduwin and Yudistira (2021) to invert Rayleigh wave dispersion curve to obtain shear wave velocity. In the initial step, we gave initiation (H and V_s search space model) in Table 1. The second step is generating particles or individuals as many as n-particle (n = 100), which value of each individual (H and V_s values) will be inside the search space model that has been determined. The next step is to calculate the HVSR curve value (forward model) theoretically. In this forward model calculation, we used the code in Open HVSR (Bignardi et al., 2016; Bignardi et al., 2017). From the result of that theoretical model, its objective function value will be calculated using norm-2 $\boldsymbol{L_2}$: $\|\boldsymbol{e}\|_2 = \left(\sum_{i=1}^{N} |\boldsymbol{e_i}|^2\right)^{1/2}$, where N is the number of data and e is i-th data. The minimum objective function value will be selected to determine the l and g parameters (particle's best position and particles in the group). The last step calculates the particle's velocity value (V) and position ($\boldsymbol{X}$). A particle with a high objective function value will move and adjust according to its V and $\boldsymbol{X}$ with a minimum objective function value. Meanwhile, the particle with minimum objective function value will be in its position until found by other particles with the minimum objective function value.

To compare how good this PSO algorithm works, we tried to compare it with a genetic algorithm (GA). The tuning parameter that we used in GA includes cross-over length 0.5 and probability of mutation of 0.15. The parameter that we will estimate in this inversion process is V_s velocity value and layer thickness. On the other side, body waves velocity (V_p) and density (ρ) are estimated using an empirical equation derived by (Brocher, 2005).

$$V_P = 0,9409 + 2,0947V_s - 0,8206V_s^2 + 0,2683V_s^3 + 0,0251V_s^4 \quad (9)$$

$$\rho = 1,6612V_p - 0,4721V_p^2 + 0,0671V_p^3 - 0,0043V_p^4 + 0,000106V_p^5 \quad (10)$$

where the unit of velocity is in km/s and density is in g/cm^3.

4. Numerical simulation using synthetic examples

This section applied an inversion method simulation with the PSO and GA algorithm on two types of synthetic data, where the first type is performed without noise. Meanwhile, the second type is contaminated by 10% of random noise. These things are intended to determine how far PSO and GA algorithms work to obtain the best solution close to its synthetic model. Synthetic model consists of 5 layers model with the thickness of parameter H_1 = 10 m, H_2 = 15 m, H_3 = 20 m, H_4 = 25 m, and H_5 = 25 m. meanwhile for the shear waves velocity parameter V_{s1} = 100 km/s, V_{s2} = 200 km/s, V_{s3} = 450 km/s, V_{s4} = 600 km/s, and V_{s5} = 800 km/s.

The inversion process is performed by generating 100 particles and 100 iterations. Thus, there will be 10,100 forward models in PSO inversion where the minimum value of the objective function will be evaluated and calculated. Meanwhile, the total number of forwarding models calculated will differ based on the given cross-over length value and the mutation probability in GA inversion. The more significant the given value the more individuals encounter cross-over and mutation. With more individuals generated, it will cause computation time to increase, so the opposite.

Table 1. Inversion result of synthetic data using PSO and GA algorithm and its SD value.

Parameter	True model	Search space	PSO inversion		GA inversion	
			Noise-free	Noise 10%	Noise-free	Noise 10%
H_1 (m)	10	5–30	10.44 ± 0.78	10.49 ± 0.72	10.01 ± 1.31	10.91 ± 1.29
H_2 (m)	15	5–30	15.25 ± 0.75	15.06 ± 0.82	14.00 ± 1.49	15.89 ± 1.69
H_3 (m)	20	5–30	21.78 ± 0.96	22.19 ± 0.98	24.01 ± 1.70	28.82 ± 2.84
H_4 (m)	25	5–30	21.81 ± 0.67	25.97 ± 0.55	21.01 ± 1.25	27.38 ± 1.31
H_5 (m)	25	5–30	22.83 ± 0.55	24.35 ± 0.47	21.02 ± 1.16	25.10 ± 0.86
Vs_1 (m/s)	100	50–300	104.75 ± 11.09	104.53 ± 11.93	101.00 ± 17.64	105.47 ± 16.15
Vs_2 (m/s)	200	100–500	203.12 ± 10.69	202.68 ± 9.17	182.01 ± 17.07	219.28 ± 13.56
Vs_3 (m/s)	350	100–500	374.09 ± 12.26	392.04 ± 8.94	393.00 ± 12.85	378.62 ± 19.79
Vs_4 (m/s)	500	250–1500	488.81 ± 18.24	534.31 ± 24.93	472.01 ± 23.90	754.04 ± 57.19
Vs_5 (m/s)	800	500–1500	842.30 ± 25.65	808.06 ± 23.87	915.00 ± 51.94	947.57 ± 61.69
Misfit			0.0437	0.1610	0.1267	0.2063
SI (%)			94.288	91.133	89.904	83.848

The best model can be chosen using a simple statistic method on posterior data distribution that resulted during the iteration process, which solution can be selected by calculating mean value, median, or mode from an available aggregate of models. According to Gonzales and Ottenbacher (2001) and Manikanda (2011) research, by using mean value, the data existence that deviated from the posterior trend (outliers) will cause the solution to keep the distance from its actual value. However, if solution choice is performed using mode value and the detailed data are very little, the solution cannot represent the available posterior distribution. Therefore, all the data do not have a single-mode value, and even some do not have it.

Meanwhile, with median, always in-between average value and mode. In addition, the median is not affected by the presence of outliers, which means that the posterior distribution represents all values. The solution selection also can be performed by choosing an individual with the most minimum objective function value from all the generated individuals during the iteration process. Farduwin and Yudistira (2021) presented a statistical method (mean and median value) to choose the best model parameters. The result shows that in the iteration >20, for each iteration process the using median value will have the same error value as using the model parameter that was selected from the most minimum objective function value. This indicates that all models have moved in the same direction. In this research, we choose the best model parameters using minimum misfit from all model parameters resulted during iteration process and calculated standard deviation (SD), both for PSO or GA.

Table 1 performs the inversion result between noise-free data and 10% random noise-contaminated data. PSO inversion shows a closer value to its actual model than GA inversion for noise-free data or data with noise. The layer thickness (H) from PSO and GA inversions result have a relatively similar value, while velocity value V_s is quite different, especially on the third to fifth layer. This thing caused by the H parameter's search space model being narrower than the velocity V_s value search space model, which is more extensive. Figures 1a–1b show that PSO inversion is closer to the synthetic HVSR curve rather than GA Inversion. This thing also can be seen in Figures 1e–1f**,** which shows the most minimum objective function value (misfit) with PSO inversion. From that error curve, it can be concluded that PSO inversion is faster toward the minimum objective value than GA. Starting from iteration >20, the model was already heading to convergent. GA inversion gave a higher misfit value and needed many iterations to obtain a misfit value similar to PSO. PSO inversion can reach a minimum misfit of 0.0437 in noise-free data conditions. Meanwhile, GA inversion gave 0.1267. PSO inversion has a misfit of 0.1610 in noise-

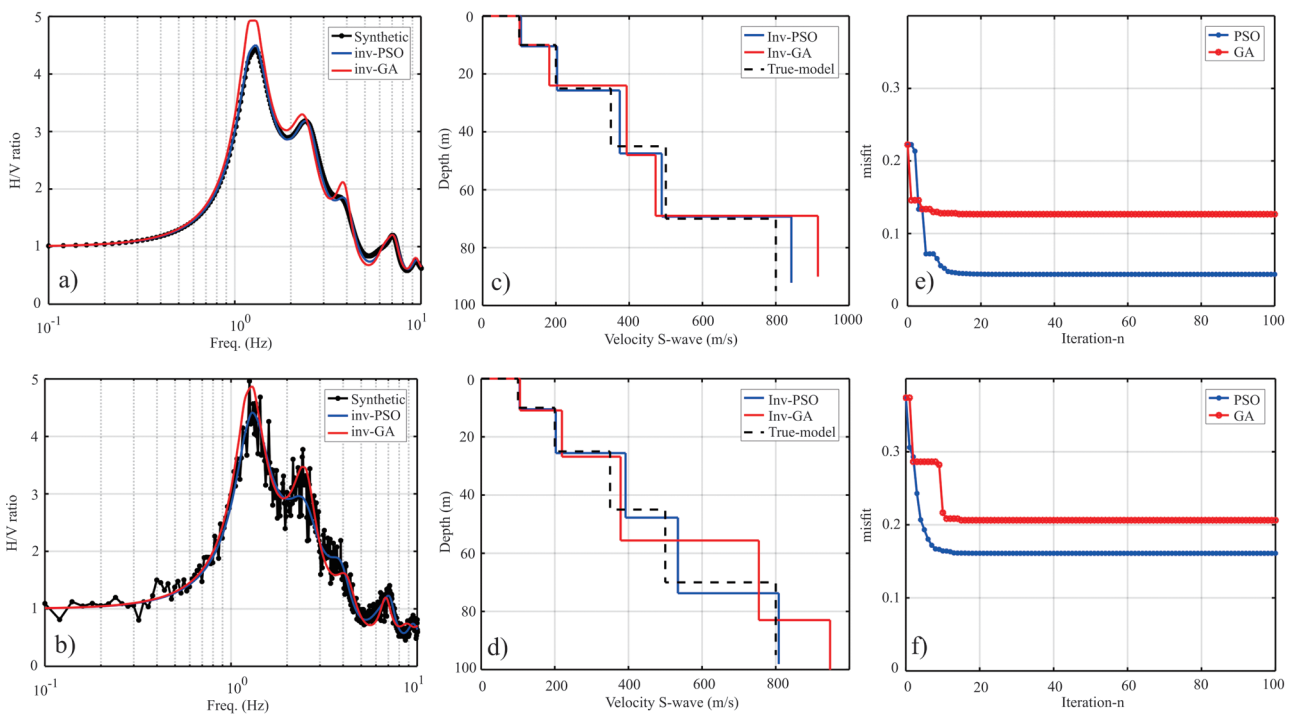

Figure 1. PSO and GA inversion result of synthetic data. (a,c,e) HVSR curve, earth layers model, and error curve of free noise synthetic data; (b,d,f) HVSR curve, earth layers model, and error curve of 10% random noise synthetic data.

contaminated data, and GA inversion has 0.2063. Thus, the PSO algorithm is fast heading to convergent, relatively stable, and resistant to noise rather than GA.

To see how close the result solution from an inversion with the actual model, we did similarity index (SI) calculation that was also used by (Laby et al., 2016) with the equation as follows:

$$SI = \left(1 - \frac{\sum_m^M \frac{\left| p_m^{inv} - p_m^r \right|}{p_m^r}}{M} \right) x\ 100\% \quad (11)$$

The SI value of about 1%–100%. p_m^{inv} is the model parameter of inversion result, and p_m^r is the actual model parameter, and M is the number of layers.

Figures 1c–1d show the layer model comparison from each inversion algorithm with its actual model. PSO inversion gave an SI value of 94.288%, while GA inversion was 89.908% in the noise-free data. In noise-contaminated data, PSO inversion can come up to its actual model with an SI value of 91.133%, and GA inversion has an SI value of 83.848%. A significant SI value shows that the inversion result solution is getting like the actual data. Even though noise-free data, especially velocity value on the fifth layer, shows fewer fits with the actual data. However, the result was better and closer than GA with the PSO algorithm. While in the noise-contaminated data, the PSO inversion result gave a relatively close result rather than GA that gave a more significant value, especially thickness and velocity value in the fourth and fifth layer.

Overall, a solution that gets close to the actual model value can be performed by multiplying the number of particles. For example, the raised particles can make the search space model more explored. However, increasing the number of particles or iteration will make computation time longer. By paying attention to the result from synthetic data inversion, we choose the particle number of 100 and iteration of 100 times. The PSO algorithm is fast heading to the concurrent and does not need iteration.

5. The Way Baka fault modeling

This section applied a methodology to the Way Baka fault area for HVSR curve inversion located in the Bakauheni district and the southern part of Sumatera Island, Indonesia. Sumatera is located in the southwest segment of the Eurasian plate that mashed up convergently by the Indo-Australian plate. It formed a subduction area across the border (McCaffrey, 2009). The subduction of the Indo-Australian plate to the Eurasian plate moves with a relative velocity of 6–7cm/year (Simandjuntak and Barber, 1996). That condition implies forming interesting geological structures, especially the Semangko Fault that sweeps from Aceh (north end of Sumatera) to Lampung (south end of Sumatera). Semangko Fault is a right-lateral strike-slip fault that moves obliquely to the northwest (Sieh and Natawidjaja, 2000). Bakauheni is located <400 km from the earthquake source lane oblique between the Indo-Australian Plate and the Eurasian plate, located <200 km from the earthquake lane of Mentawai active fault, 100 km from the earthquake lane of Semangko Fault. Sadewo et al. (2013) studied morph structure and paleoseismic in the Bakauheni area and its surroundings by analyzing satellite imaging of DEM SRTM (Digital Elevation Model Shuttle Radar Topography Mission). Geological kinematics structure analysis shows an active potential fault in the Way Baka area, a left-lateral strike-slip fault with direction U185°T/74° with the main force U165°T. Paleoseismic study along Way Baka Fault shows that tectonic activity has occurred since the Plio-Pleistocene period (±3 million years ago.).

5.1. HVSR measurement and inversion

The microtremor data in this research was recorded using three components of seismograph in 7 location measurement points (Figure 2) with sampling time of 0.01 s and length of measurement about 25–30 min. On ambient noise signal recording in a site, often affected by human activities, wind, and drift from the instrument itself or usually called with noise. Therefore, the measurement parameter on the field should be determined to reduce unwanted disruption. The wind effect and drift from the instrument can be reduced by waveform filtering with two orders Butterworth filter with frequency cutoff about 0.3 Hz. HVSR accuracy escalation, the signal is separated into a low and high-level noise section (Mihaylov et al., 2016).

We used Geopsy and Octave software on the process to obtain the HVSR curve. The processing parameter we used is a range frequency filter of 0.5–15 Hz and window length 30 s. Then we applied the antitrigger algorithm to erase the transient signal or signal with very low amplitude (STA = 1s; LTA = 30s) with STA/LTA between 1.0–3.5. Finally, we used a smoothing filter to erase the modulation effect and spike with extreme value on the HVSR curve (Konno and Ohmachi, 1998).

Figure 3 shows the result of the HVSR curve for all selected windows in AWB1, AWB2, AWB3, and AWB6 points. The black curve is an average HVSR curve from all received curves in every measuring point. On AWB6 and AWB4 point, the curves resulting from windowing show a H/V ratio value that is less smooth and had many surges on 1–10 Hz frequency. We estimated that anomaly is caused by a high noise related to a densely populated village area. The HVSR average curve on every point is then used for the inversion process using the RR-PSO algorithm (eq. 8) to estimate velocity value V_s. The number of layers used during the inversion is 5 layers. This refers to Farduwin et al. (2021) who carried out electrical resistivity tomography (ERT) measurements near the research study

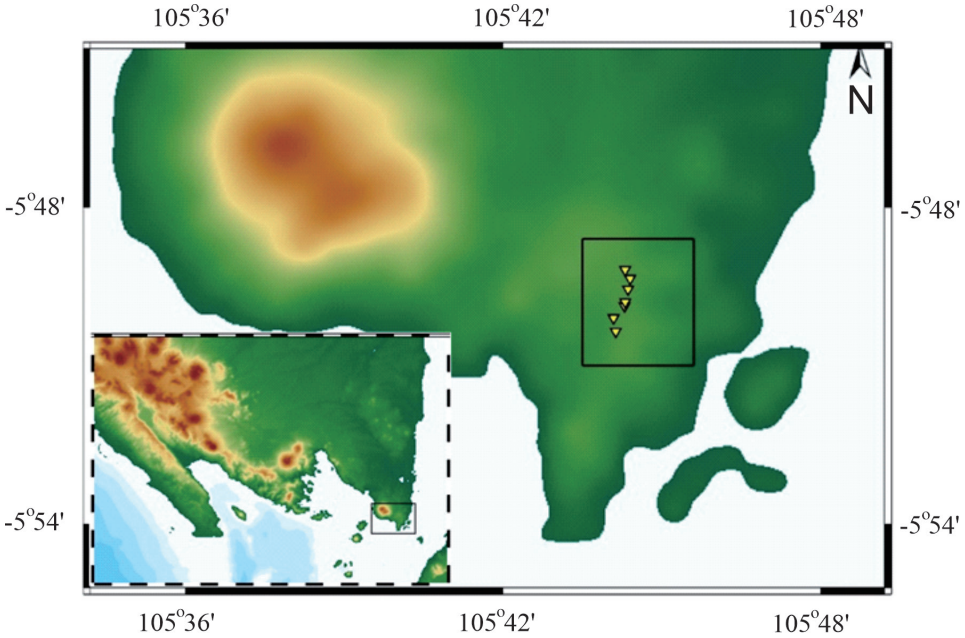

Figure 2. Location map of microtremor measurement in Way Baka fault, Bakauheni district, Indonesia. Yellow inverted triangles indicate stations.

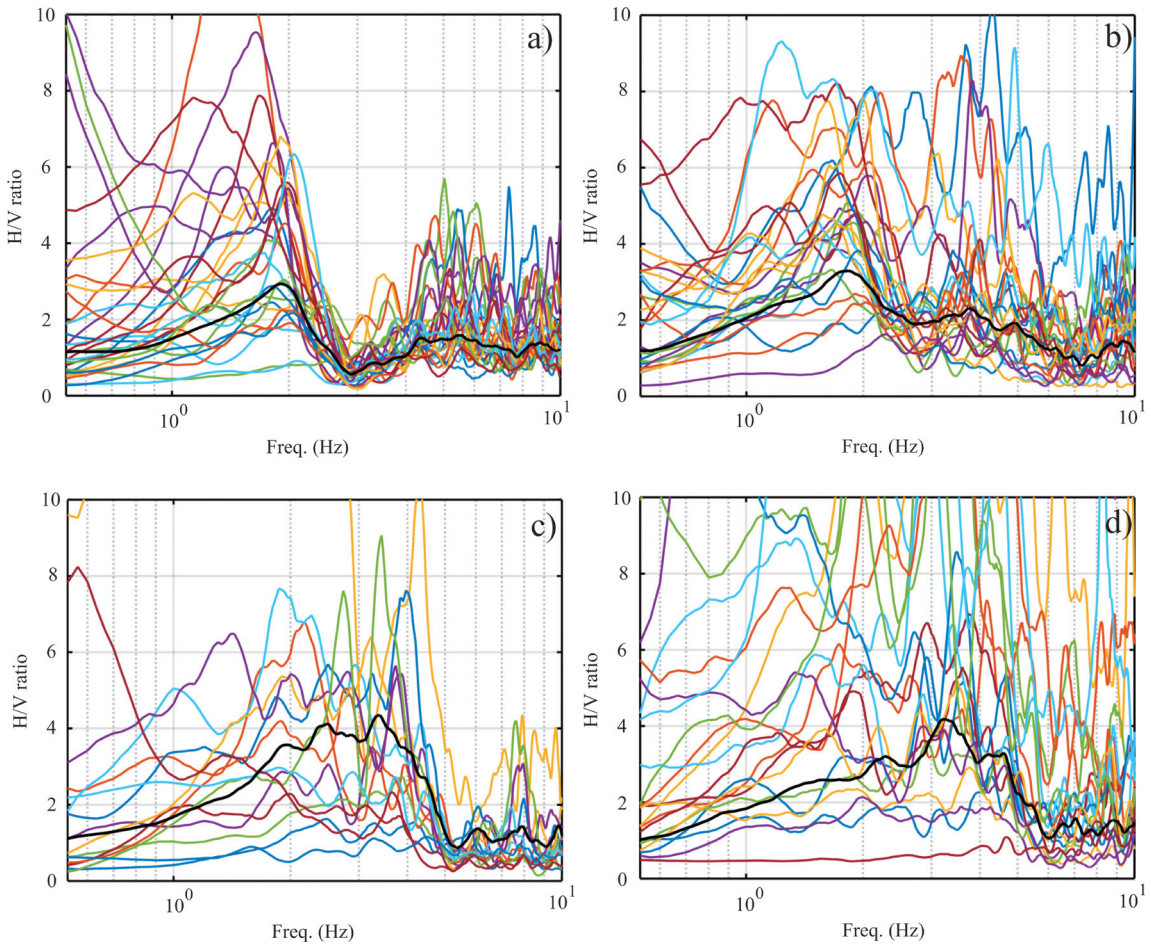

Figure 3. HVSR curve produces from record length about 25–30' at measurement point (a) ABW1; (b) ABW2; (c) ABW4; (d) ABW6.

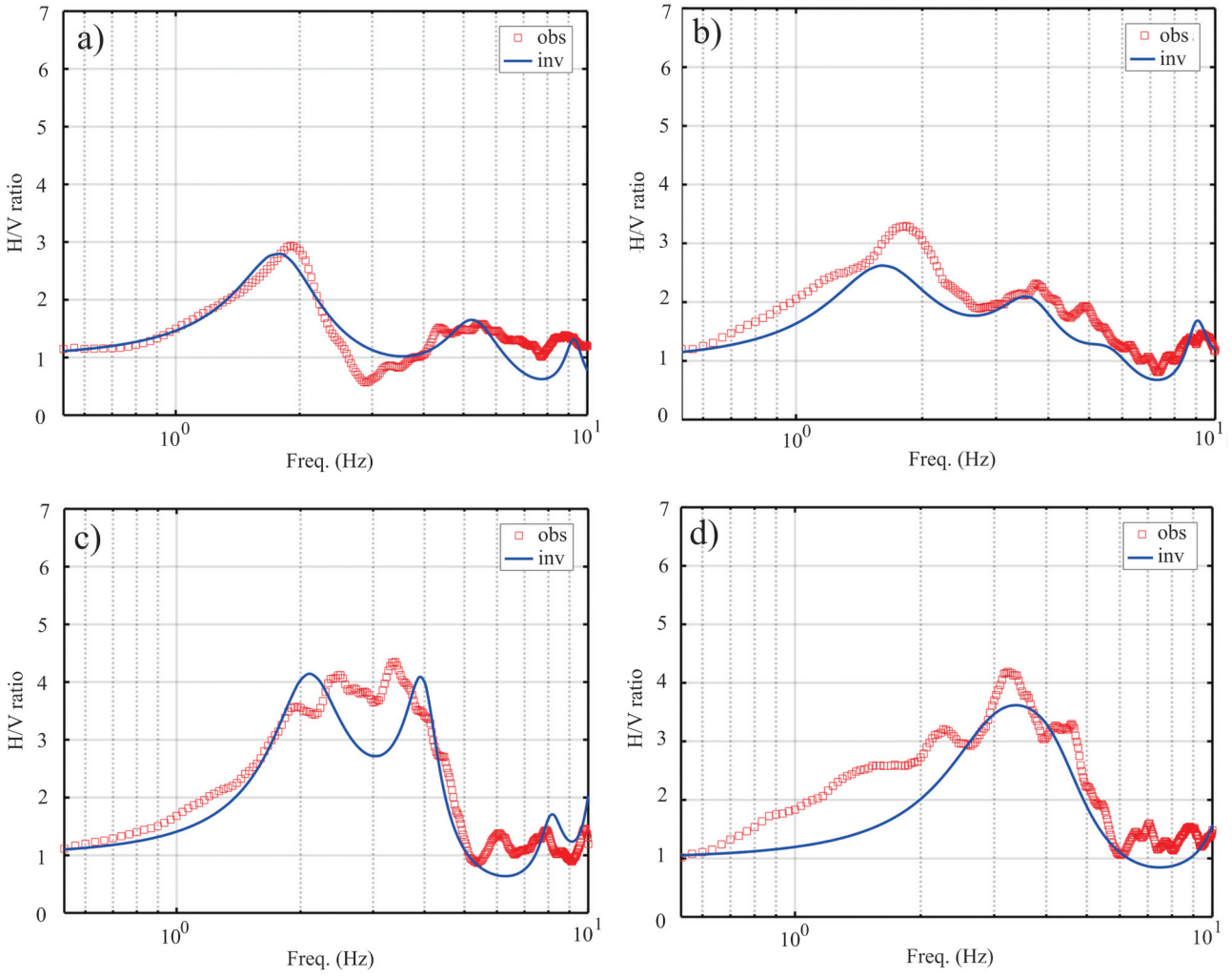

Figure 4. HVSR curve resulted from PSO inversion. Red square is observed data, and blue line is inversion result (a) ABW1; (b) ABW2; (c) ABW4; (d) ABW6.

which showed that there were three main layers in the site to a deep of 40– 60 m. For a deeper depth (up to 100 m), we add two layers below it.

PSO inversion result shows the HVSR curve is relatively close to the HVSR observation curve (Figure 4), but at some sites not too close to an observed inversion result. This is caused by the higher noise level in those sites caused by human activity (near with highway and industrial machine). The misfit value is relatively small for all sites, about 0.33–0.6 (Figure 5). Table 2 presents the model parameters value that was chosen from the minimum misfit value and its SD for each model parameters. This matter showed a relatively small misfit value of about 0.33–0.6 (Figure 5). The error curve also indicates that PSO is swift, converging on the twentieth iteration. The inversion result model has been relatively stable on minimum objective function value. This matter shows that posterior model distribution with PSO inversion moved to the point with the minimum objective function value on the twentieth iteration. Figure 6 is the model per layer of PSO inversion result, which model solution chosen with minimum misfit value (red line). At the same time, the model from each iteration (black line) shows that the model still has a high solution value in the initial iteration. The model is moved to one point (with the lowest misfit). Based on all the model results, it can be seen that the area around the Way Baka fault has a per layer model where the V_s velocity value becomes more significant with increasing depth. However, the fifth layer on AWB1 and AWB4 points show a lower velocity value than the layer over it.

5.2. Shear wave velocity estimation

The microtremor measurement track obtains three intersection points with the Way Baka fault. The three points are marked with the symbol Cs (Cross Section) as the location of the fault crossing (Figure 7). The location of the Cs1 point is between the acquisition points AWB1

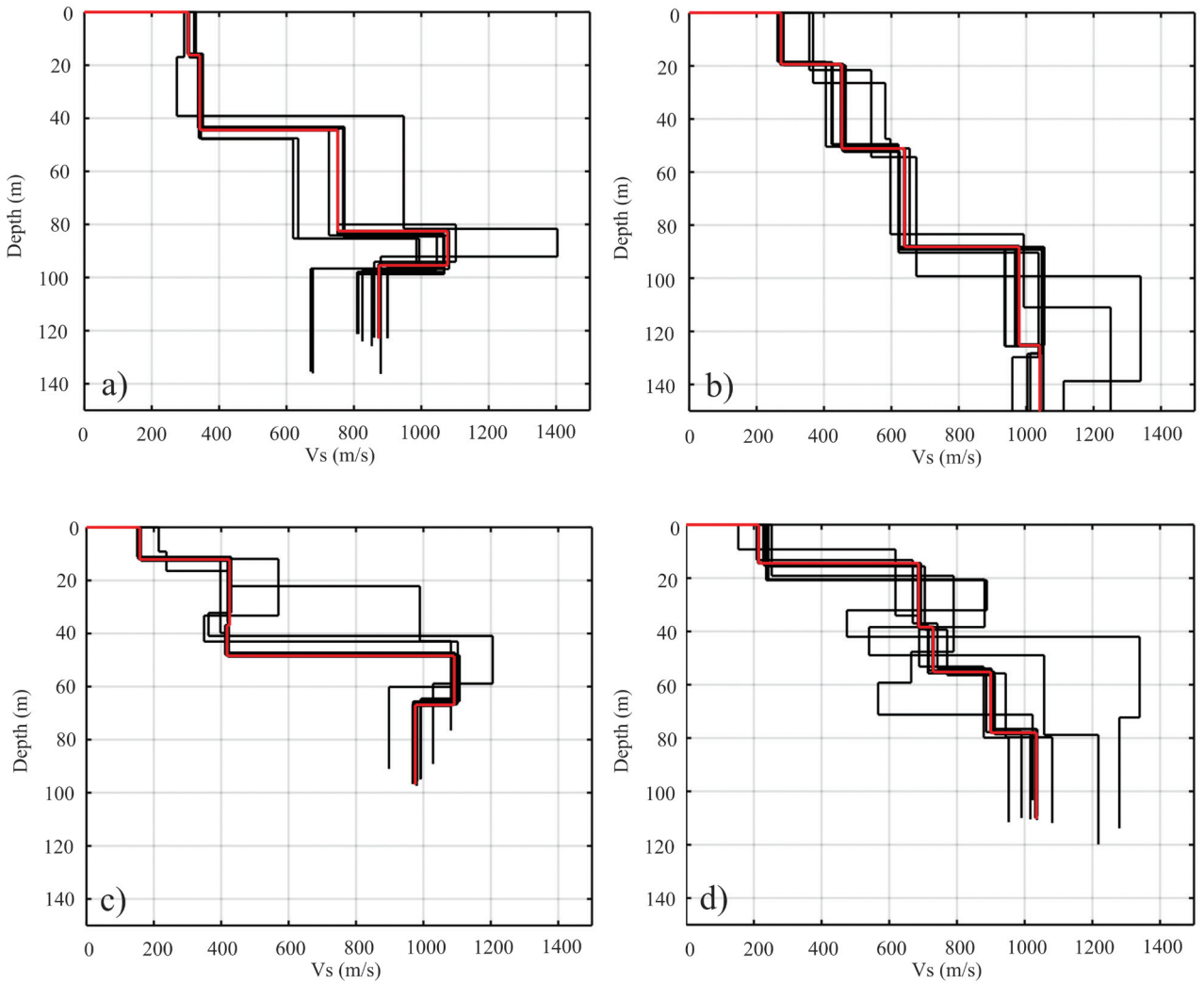

Figure 5. Earth layers model resulted from PSO inversion; (a) ABW1; (b) ABW2; (c) ABW4; (d) ABW6. Redline is the best inversion model chosen using minimum misfit from all posterior data. The black line is the best model at each iteration.

Table 2. Inversion result of observed data using PSO and its SD value.

Parameter	Site						
	AWB1	AWB2	AWB3	AWBP	AWB4	AWB5	AWB6
H_1 (m)	16.21 ± 6.81	19.40 ± 6.16	7.51 ± 2.31	21.88 ± 4.95	12.13 ± 2.35	16.52 ± 3.33	14.42 ± 2.42
H_2 (m)	28.19 ± 5.95	31.72 ± 5.23	8.79 ± 2.07	24.16 ± 5.99	24.77 ± 3.38	23.91 ± 5.66	23.97 ± 4.33
H_3 (m)	38.10 ± 6.99	37.04 ± 5.08	15.46 ± 5.25	26.52 ± 4.46	11.49 ± 2.62	21.58 ± 5.02	16.82 ± 5.06
H_4 (m)	12.88 ± 6.26	37.11 ± 5.96	31.08 ± 4.49	23.29 ± 4.45	18.51 ± 4.67	35.31 ± 5.51	22.77 ± 5.01
H_5 (m)	27.64 ± 6.95	40.49 ± 5.43	17.28 ± 5.35	22.72 ± 5.29	30.01 ± 4.73	37.21 ± 6.12	32.38 ± 4.60
Vs_1 (m/s)	308.44 ± 51.68	272.38 ± 61.5	184.60 ± 53.3	245.46 ± 53.22	158.44 ± 36.75	145.38 ± 30.31	213.98 ± 36.65
Vs_2 (m/s)	342.61 ± 43.22	452.91 ± 62.31	472.33 ± 31.9	537.66 ± 11.37	424.79 ± 20.62	559.21 ± 43.05	686.47 ±60.35
Vs_3 (m/s)	751.74 ± 44.37	639.04 ± 11.22	568.73 ± 10.96	759.13 ± 28.03	417.19 ± 30.19	517.88 ± 59.32	729.51 ± 39.38
Vs_4 (m/s)	1077.65 ± 20.12	979.17 ± 17.39	976.97 ± 51.71	944.96 ± 47.83	1091.15 ± 76.67	812.90 ± 89.61	899.69 ± 63.05
Vs_5 (m/s)	873.96 ± 69.5	1040.33 ± 69.4	1131.06 ± 89.75	1067.07 ± 76.40	975.61 ± 66.87	1169.30 ± 94.76	1034.59 ± 54.05

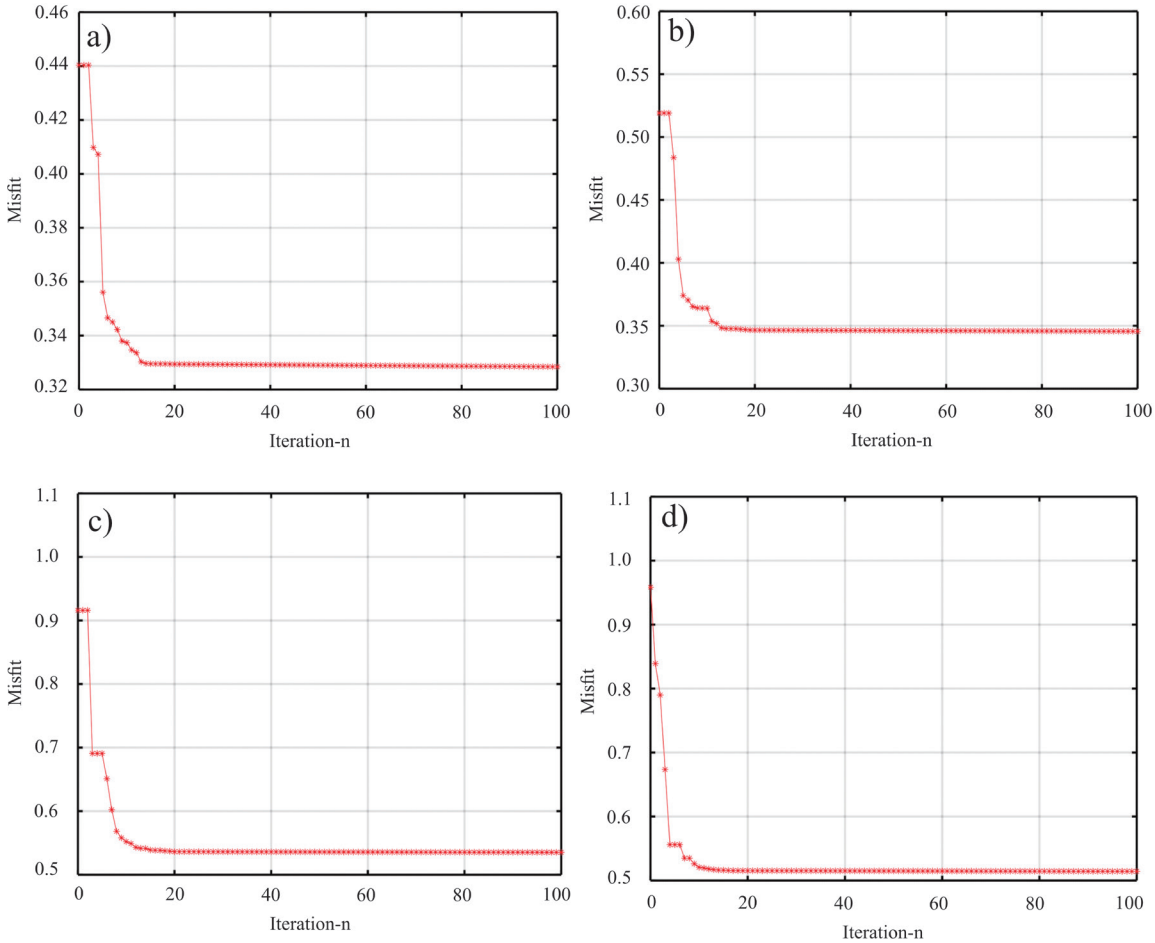

Figure 6. Error curve resulted from PSO inversion; (a) ABW1; (b) ABW2; (c) ABW4; (d) ABW6.

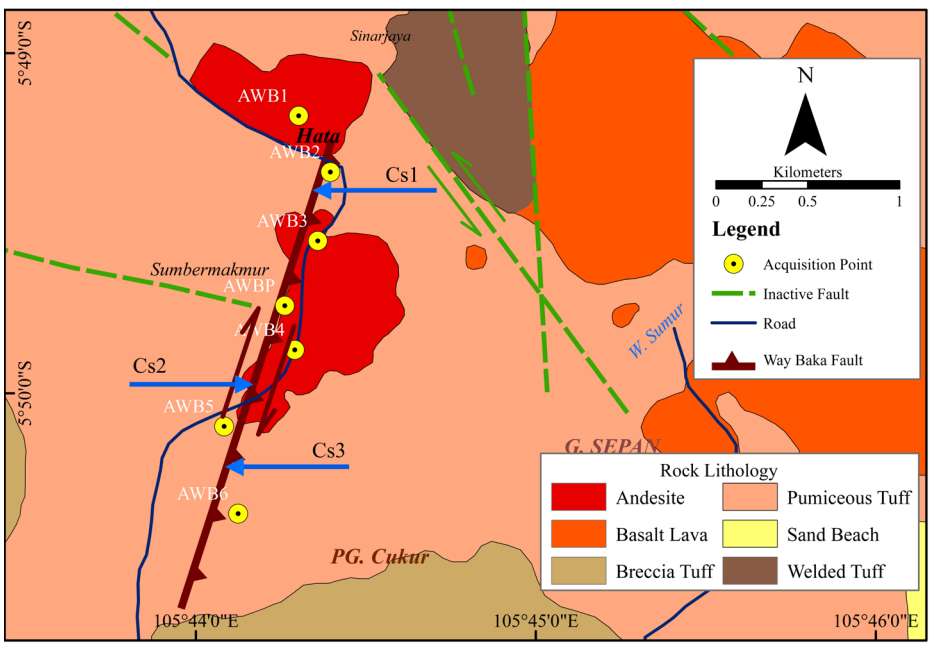

Figure 7. Microtremor measurement path intersecting with Way Baka fault at three cross-section points (Cs) (Mangga et al., 1993).

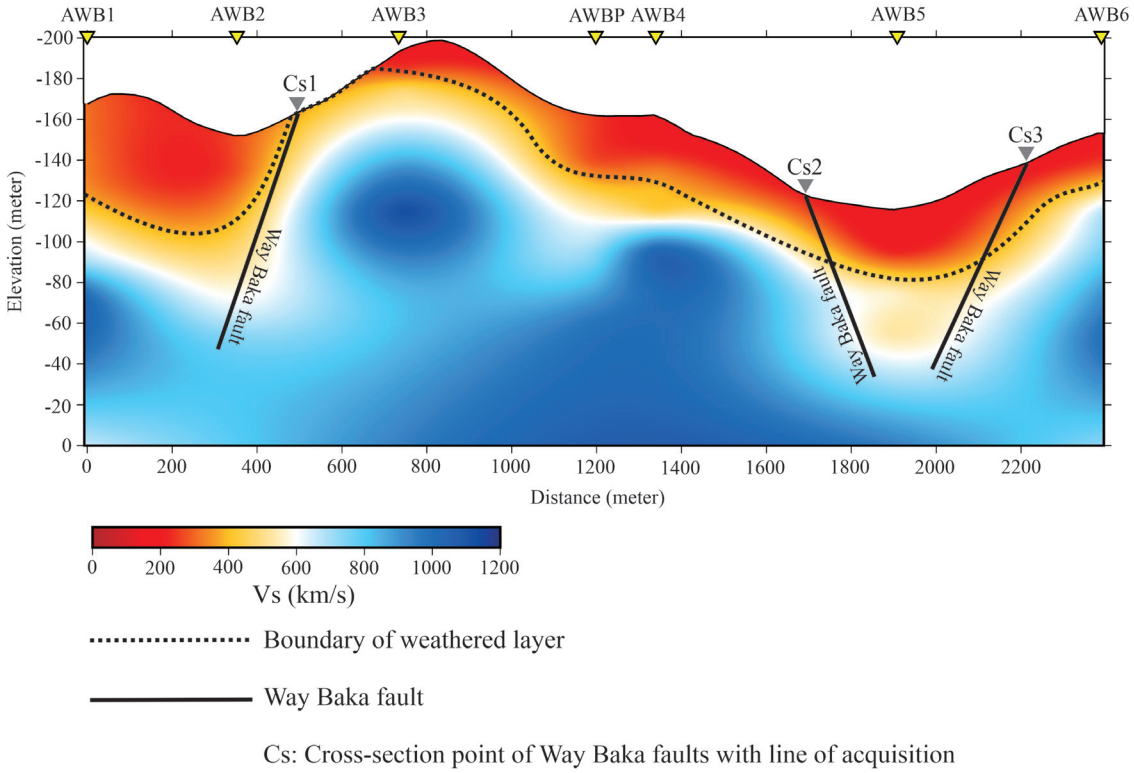

Figure 8. The interpretation of the Way Baka Fault existence in 2D cross-section of microtremor data inversion results at the study site. The yellow triangle with the AWB label indicates the microtremor measurement point, while the gray triangle with the Cs label indicates the intersection point with the fault.

to AWB3. The section crosses between two hills with a dominant lithology of andesite rocks. In addition, there is a valley with pyroclastic rocks dominated by pumiceous tuff in the middle.

Meanwhile, the intersection points of Cs2 and Cs3 are on the section between AWB4, AWB5, and AWB6 points. Pyroclastic rocks dominate the rock layer at this location in the form of pumiceous tuff. Topographically, the area of this intersection tends to be lower than the first point. These three intersection points (Cs) are aligned with the cross-section of the inversion velocity V_s, which shows the fault pattern.

The velocity pattern is obtained based on the inversion result, indicating Way Baka Fault's presence (Figure 8). At the first point of intersection (Cs1), there is a pattern of the continuous velocity of weathered rock layers from a depth of –80 m to –160 m. This interpretation is linear, with significant geomorphological changes in steep slopes accompanied by many remnants of landslides. However, a weathered rock layer affected a bridge collapse on the highway. This condition contrasts in weathering layer thickness between AWB1 and AWB3 points 10 to 40 m in-depth.

The intersection points of Cs2 and Cs3 also show a fault pattern, especially in the center of softening at the AWB5 point. The pattern of noncontinuity in these sections characterizes the contrasting changes in velocity related to weathered rocks that fill the area. The Way Baka faults show the same slope pattern in the two-velocity section. The direction of the Cs2 section that is northeast to southwest crosses AWB4 and AWB5. At the same time, the Cs3 section is northwest from AWB5 to the southeast to AWB6 point. Based on surface observations, the fault plane in this area is not apparent. However, this region is relatively flat with a few low hills due to geomorphology.

The findings of the fault plane pattern on the results of the microtremor wave inversion corroborate the results of this study about the existence of the Way Baka fault plane. These results are also consistent with previous paleo-seismic research. The alignment of these findings reinforces the presence of the Way Baka Fault in the Bakauheni area and its surroundings as active potential faults. The noncontinuous pattern in the cross-section of the inversion results that characterize changes in rock lithology strengthen the indication of the Way Baka fault area. The appropriateness of the location of the intersection of the measurement path and fault pattern reinforces this interpretation.

However, these results still require further research with other methods to ascertain the characteristics and

other properties of the Way Baka fault. Go forward, and it is necessary to make more detailed measurements related to the direction of the strike and dip from the fault plane and the offset distance of the bedding on the axis of the fault plane to ascertain the Way Baka fault type. In addition, monitoring seismic activity at the fault site is also essential to ensure disaster mitigation efforts related to the seismic process and reactivation of faults in the Bakauheni and surrounding areas.

6. Conclusion

The HVSR curve inversion with the RR-PSO algorithm was used to process and obtain velocity V_s estimation for the subsurface modeling. This algorithm is shown with performing analysis on synthetic data (noise-free and 10% random noise-contaminated) and actual data. The results from the synthetic tests show acceptable results and came up with a real solution. The advantage of the PSO algorithm is that it can be used for various inversion problems without being equipped with a priori information first.

The PSO application on actual data shows a significant result. For example, a 2D velocity V_s section can show sediment layers, basement layers, and fault planes in Way Baka. This result concluded that the inversion method with the PSO algorithm could be developed for geological hazard mitigation based on ambient noise data, especially HVSR data.

Conflict of interest

The author(s) declare(s) that there is no conflict of interest regarding the publication of this article.

Acknowledgment

The authors are thankful to the Kemendikbudristek Indonesia that has fully funded this research based on PDUPT 2022 program with contract numbers 114/E5/PG.02.00.PT/2022 and 2147/UN26.21/PN/2022. Likewise, thanks to Geophysical Engineering Department Universitas Lampung for providing a laboratory to carry out this research work.

References

1. Aki K, Richards PG (2002). Quantitative Seismology, 2nd Ed. In University Science Books 68 (5).
2. Akkaya İ (2015). The application of HVSR microtremor survey method in Yüksekova (Hakkari) region, Eastern Turkey. Journal of African Earth Sciences 109: 87–95.
3. Akkaya İ, Özvan A (2019). Site characterization in the Van settlement (Eastern Turkey) using surface waves and HVSR microtremor methods. Journal of Applied Geophysics 160: 157–170.
4. Asten M (1978). Geological control on the three-component spectra of Rayleigh-wave microseisms. Bulletin of the Seismological Society of America 68 (6): 1623–1636.
5. Bignardi S, Mantovani A, Zeid NA (2016). OpenHVSR: Imaging the subsurface 2D/3D elastic properties through multiple HVSR modeling and inversion. Computers and Geosciences 93: 103–113.
6. Bignardi S, Yezzi AJ, Fiussello S, Comelli A (2018). OpenHVSR - Processing toolkit: Enhanced HVSR processing of distributed microtremor measurements and spatial variation of their informative content. Computers and Geosciences 120: 10–20.
7. Bignardi S, Zeid NA, Corradini E, Santarato G (2017). The HVSR technique from array data, speeding up mapping of paleo-surfaces and buried remains. The case of the Bronze-Age site of Pilastri (Italy). SEG Technical Program Expanded Abstracts 36: 5119–5124.
8. Bonnefoy-Claudet S, Cornou C, Bard PY, Cotton F, Moczo P et al. (2006). H/V ratio: A tool for site effects evaluation. Results from 1-D noise simulations. Geophysical Journal International 167 (2): 827–837.
9. Brocher TM (2005). Empirical relations between elastic wavespeeds and density in the Earth's crust. Bulletin of the Seismological Society of America 95 (6): 2081–2092.
10. D'Amico V, Picozzi M, Baliva F, Albarello D (2008). Ambient noise measurements for preliminary site-effects characterization in the Urban area of Florence, Italy. Bulletin of the Seismological Society of America 98 (3): 1373–1388.
11. Ding Y, Zhang W, Yu L, Lu K (2019). The accuracy and efficiency of GA and PSO optimization schemes on estimating reaction kinetic parameters of biomass pyrolysis. Energy 176: 582–588.
12. Ekinci YL, Balkaya Ç, Göktürkler G (2019). Parameter estimations from gravity and magnetic anomalies due to deep-seated faults: Differential evolution versus particle swarm optimization. Turkish Journal of Earth Sciences 28 (6): 860–881.
13. Essa KS, Elhussein M (2020). Interpretation of Magnetic Data Through Particle Swarm Optimization: Mineral Exploration Cases Studies. Natural Resources Research 29 (1): 521–537. https://doi.org/10.1007/s11053-020-09617-3
14. Farduwin A, Lumbatoruan PG, Karyanto, Triyanto D (2021). Identification of zeolite using electrical resistivity tomography in Campang Tiga, South Lampung Regency. IOP Conference Series: Earth and Environmental Science 882 (1).
15. Farduwin A, Yudistira T (2021). Shear velocity inversion from ambient seismic noise using RR-PSO: A case study of Nusa Tenggara Island. Journal of Physics: Conference Series 1949 (1).

16. Fernández-Martínez JL, García-Gonzalo E, Fernández-Álvarez JP, Kuzma HA, Menéndez-Pérez CO (2010). PSO: A powerful algorithm to solve geophysical inverse problems Application to a 1D-DC resistivity case. Journal of Applied Geophysics 71 (1): 13–25.

17. Fernández-Martínez JL, GarcÍa-Gonzalo E (2012). Stochastic stability and numerical analysis of two novel algorithms of the PSO family: PP-GPSO and RR-GPSO. International Journal on Artificial Intelligence Tools 21 (3).

18. Gallipoli MR, Mucciarelli M, Gallicchio S, Tropeano M, Lizza C (2004). Horizontal to vertical spectral ratio (HVSR) measurements in the area damaged by the 2002 Molise, Italy, earthquake. Earthquake Spectra 20 (1).

19. Gallipoli MR, Stabile TA, Giulia M, Zaeid NA, Leonardo C et al. (2018). Ambient Vibration Tests on a Building Before and After the 2012 Emilia (Italy) Earthquake. 16th European Conference on Earthquake Engineering (16ECEE): 1–10.

20. García-Jerez A, Piña-Flores J, Sánchez-Sesma FJ, Luzón F, Perton M (2016). A computer code for forward calculation and inversion of the H/V spectral ratio under the diffuse field assumption. Computers and Geosciences 97: 67–78.

21. Godio A, Santilano A (2018). On the optimization of electromagnetic geophysical data: Application of the PSO algorithm. Journal of Applied Geophysics 148: 163–174.

22. Göktürkler G, Balkaya Ç (2012). Inversion of self-potential anomalies caused by simple-geometry bodies using global optimization algorithms. Journal of Geophysics and Engineering 9 (5): 498–507.

23. Gonzales VA, Ottenbacher KJ (2001). Measures of central tendency in rehabilitation research: What do they mean? American Journal of Physical Medicine and Rehabilitation 80 (2): 141–146.

24. Guéguen P, Cornou C, Garambois S, Banton J (2007). On the limitation of the H/V spectral ratio using seismic noise as an exploration tool: Application to the Grenoble valley (France), a small apex ratio basin. Pure and Applied Geophysics 164 (1): 115–134.

25. Gutenberg B (1936). On Microseismics. Bulletin of the Seismological Society of America 69: 111–117.

26. Harutoonian P, Leo CJ, Tokeshi K, Doanh T, Castellaro S et al. (2013). Investigation of dynamically compacted ground by HVSR-based approach. Soil Dynamics and Earthquake Engineering 46: 20–29.

27. Herak M (2008). Model HVSR-A Matlab tool to model horizontal-to-vertical spectral ratio of ambient noise. Computers & Geosciences 34: 1514–1526.

28. Kennedy J, Eberhart R (1995). Particle Swarm Optimisation. IEEE International Conference on Neural Networks Proceedings 4 (7).

29. Khalili M, Mirzakurdeh AV (2019). Fault detection using microtremor data (HVSR-based approach) and electrical resistivity survey. Journal of Rock Mechanics and Geotechnical Engineering 11 (2): 400–408.

30. Konno K, Ohmachi T (1998). Ground-motion characteristics estimated from spectral ratio between horizontal and vertical components of microtremor. Bulletin of the Seismological Society of America 88 (1): 228–241.

31. Laby DA, Sungkono, Santosa BJ, Bahri AS (2016). RR-PSO: Fast and robust algorithm to invert Rayleigh waves dispersion. Contemporary Engineering Sciences 9 (13–16): 735–741.

32. Lunedei E, Albarello D (2010). Theoretical HVSR curves from full wavefield modelling of ambient vibrations in a weakly dissipative layered Earth. Geophysical Journal International 181 (2): 1093–1108.

33. Lunedei E, Malischewsky P (2015). A Review and Some New Issues on the Theory of the H/V Technique for Ambient Vibrations. In Perspectives on European Earthquake Engineering and Seismology; Springer International Publishing.

34. Mangga SA, Amirudin, Suwarti T, Gafoer S, Sidarta (1993). Peta Geologi Lembar Tanjungkarang, Sumatera, skala 1:250.000. Bandung: Badan Geologi.

35. Manikandan S (2011). Measures of central tendency: Median and mode. Journal of Pharmacology and Pharmacotherapeutics 2 (3): 214–215.

36. Mantovani A, Valkaniotis S, Rapti D, Caputo R (2017). Mapping the Palaeo-Piniada Valley, Central Greece, Based on Systematic Microtremor Analyses. Pure and Applied Geophysics 175 (3): 17.

37. Maresca R, Nardone L, Gizzi FT, Potenza MR (2018). Ambient noise HVSR measurements in the Avellino historical centre and surrounding area (southern Italy). Correlation with surface geology and damage caused by the 1980 Irpinia-Basilicata earthquake. Measurement: Journal of the International Measurement Confederation 130: 211–222.

38. McCaffrey R (2009). The tectonic framework of the sumatran subduction zone. Annual Review of Earth and Planetary Sciences 37: 345–366.

39. Mihaylov D, Naggar MH, Dineva S (2016). Separation of high- and low-level ambient noise for HVSR: Application in city conditions for Greater Toronto area. Bulletin of the Seismological Society of America 106 (5): 2177–2184.

40. Mucciarelli M, Gallipoli MR (2001). A critical review of 10 years of microtremor HVSR technique. Bollettino Di Geofisica Teorica Ed Applicata 42 (3–4): 255–266.

41. Nakamura Y (1989). A Method for Dynamic Characteristic Estimation of Surface. Quarterly Reports of The Railway Technical Research Institute, 9.

42. Nakamura Y (2000). Clear identification of fundamental idea of Nakamura's technique and its applications. Proceedings of the 12th WCEE, Paper no. 2656.

43. Nogoshi M, Igarashi T (1970). On the Propagation Characteristics of Microtremor. Journal of the Seismological Society of Japan 23 (2), 264–280.

44. Nogoshi M, Igarashi T (1971). On the amplitude characteristics of microtremor (Part 2). Journal of Seismological Society of Japan 24: 26–40.

45. Pace F, Santilano A, Godio A (2019). Particle swarm optimization of 2D magnetotelluric data. Geophysics 84 (3): E125–E141.

46. Pallero JLG, Fernández-Martínez JL, Bonvalot S, Fudym O (2017). 3D gravity inversion and uncertainty assessment of basement relief via Particle Swarm Optimization. Journal of Applied Geophysics 139: 338–350.

47. Paolucci E, Albarello D, D'Amico S, Lunedei E, Martelli L et al. (2015). A large scale ambient vibration survey in the area damaged by May–June 2012 seismic sequence in Emilia Romagna, Italy. Bulletin of Earthquake Engineering 13 (11): 3187–3206.

48. Sadewo MS, Muslim D, Soehaimi A (2013). Studi Morfostruktur dan Paleoseismik Sesar Way Baka di daerah Bakauheni, Lampung Selatan. Jurnal Lingkungan Dan Bencana Geologi 4 (1): 1–13 (in Indonesian).

49. Sánchez-Sesma FJ, Rodríguez M, Iturrarán-Viveros U, Luzón F, Campillo M et al. (2011). A theory for microtremor H/V spectral ratio: Application for a layered medium. Geophysical Journal International 186 (1): 221–225.

50. Sarkowi M, Wibowo RC, Yogi IBS, Yusuf M, Boka YS (2022). Microtremor analysis to evaluate BMKG Region III Building, Bali, Indonesia. Iranian Journal of Earth Sciences 14 (2): 104-111.

51. Scherbaum F, Hinzen KG, Ohrnberger M (2003). Determination of shallow shear wave velocity profiles in the cologne, Germany area using ambient vibrations. Geophysical Journal International 152 (3): 597–612.

52. Seht MI, Wohlenberg J (1999). Microtremor Measurements Used to Map Thickness of Soft Sediments. Bulletin of the Seismological Society of America 89 (1): 250–259.

53. Setiawan B, Jaksa M, Griffith M, Love D (2018). Seismic site classification based on constrained modeling of measured HVSR curve in regolith sites. Soil Dynamics and Earthquake Engineering 110: 244–261.

54. Sieh K, Natawidjaja D (2000). Neotectonics of the Sumatran fault, Indonesia. Journal of Geophysical Research 105 (31).

55. Simandjuntak TO, Barber AJ (1996). Contrasting tectonic styles in the neogene orogenic belts of Indonesia. Geological Society Special Publication 106 (106): 185–201.

56. Sungkono S, Santosa BJ (2011). Determine of rayleigh wave dispersion using fgrt method. Proceeding of the International Conference on Mathematics and Sciences (ICOMSc) 7.

57. Tsai NC, Housner GW (1970). Calculation of Surface Motions of a Layered Half-Space. Bulletin of the Seismological Society of America 60 (5): 1625–1651.

58. Wilken D, Wunderlich T, Majchczack B, Andersen J, Rabbel W (2015). Rayleigh-wave Resonance Analysis: a Methodological Test on a Viking Age Pit House. Archaeological Prospection 22: 187–206.

59. Zeid NA, Bignardi S, Santarato G, Peresani M (2017a). Exploring the paleolithic cave of Fumane (Italy): Geophysical methods as planning tool for archaeology. SEG Technical Program Expanded Abstracts 36: 5125–5129.

60. Zeid NA, Corradini E, Bignardi S, Nizzo V, Santarato G (2017b). The Passive Seismic Technique 'HVSR' as a Reconnaissance Tool for Mapping Paleo-soils: The Case of the Pilastri Archaeological Site, Northern Italy. Archaeological Prospection 24 (3): 245–258.

61. Zeid NA, Corradini E, Bignardi S, Morandi N, Nizzo V et al. (2016). Unusual geophysical techniques in archaeology - HVSR and induced polarization, A case history. 22nd European Meeting of Environmental and Engineering Geophysics, Near Surface Geoscience.

13% Overall Similarity

Top sources found in the following databases:

- 9% Internet database
- Crossref database
- 8% Submitted Works database
- 9% Publications database
- Crossref Posted Content database

TOP SOURCES

The sources with the highest number of matches within the submission. Overlapping sources will not be displayed.

1	**bes.ihep.ac.cn** Internet	2%
2	**skyehaven.net** Internet	<1%
3	**Benchmarking: An International Journal, Volume 21, Issue 2 (2014-03...** Publication	<1%
4	**Taibah University on 2015-05-01** Submitted works	<1%
5	**Erasmus University Rotterdam** Submitted works	<1%
6	**Istanbul Bilgi University on 2018-05-15** Submitted works	<1%
7	**Western Governors University on 2014-06-29** Submitted works	<1%
8	**edusismo.org** Internet	<1%

9	optiwave.eu Internet	<1%
10	sec.gov Internet	<1%
11	Malmros, Anna. "Advanced III-Nitride Technology for mm-Wave Applic... Publication	<1%
12	star.le.ac.uk Internet	<1%
13	media.neliti.com Internet	<1%
14	Grey Systems, Volume 2, Issue 3 (2012-10-27) Publication	<1%
15	hdl.handle.net Internet	<1%
16	Irikura, Karl K.. "Gas-Phase Energetics of Thorium Fluorides and Their I... Crossref	<1%
17	Zhe, Yan, and Gu Hanming. "Non-linear prestack seismic inversion with... Crossref	<1%
18	cgiss.boisestate.edu Internet	<1%
19	Andreas Stollwitzer, Josef Fink. "Dämpfungskennwerte des Schotterob... Crossref	<1%
20	International Journal of Managerial Finance, Volume 10, Issue 2 (2014) Publication	<1%

21	University of Strathclyde on 2018-01-28 Submitted works	<1%
22	link.springer.com Internet	<1%
23	scribd.com Internet	<1%
24	jurnal.ugm.ac.id Internet	<1%
25	Cabarrus College of Health Sciences on 2016-03-15 Submitted works	<1%
26	Guillier, Bertrand, Jean-Luc Chatelain, Sylvette Bonnefoy-Claudet, and ... Crossref	<1%
27	Indian School of Mines on 2021-05-08 Submitted works	<1%
28	dbserv.pnpi.spb.ru Internet	<1%
29	etd.adm.unipi.it Internet	<1%
30	Russell, Dalin Newell. "The Influence of Pile Shape and Pile Sleeves on ... Publication	<1%
31	University of Lincoln on 2021-02-17 Submitted works	<1%
32	doria.fi Internet	<1%

33	journals.tubitak.gov.tr Internet	<1%
34	pubs.geoscienceworld.org Internet	<1%
35	Iman Ashayeri, Arman Sadr, Mahnoosh Biglari, Ebrahim Haghshenas. "... Crossref	<1%
36	Mohammad Ali Baghapour, Mohammad Reza Shooshtarian, Mohamm... Crossref	<1%
37	Weizhang Liang, Guoyan Zhao, Suizhi Luo. "Sustainability evaluation fo... Crossref	<1%
38	pastel.archives-ouvertes.fr Internet	<1%
39	sujest.selcuk.edu.tr Internet	<1%
40	vdocument.in Internet	<1%
41	annualreviews.org Internet	<1%
42	Mirthivada, Alekhya Reddy. "A Study on Prevalence of Metabolic Syndr... Publication	<1%
43	ftp.eq.uc.pt Internet	<1%
44	sun.stanford.edu Internet	<1%

45	ftp.cpc.ncep.noaa.gov Internet	<1%
46	Alhada Farduwin, Pangeran G. Lumbatoruan, Karyanto, Dian Triyanto. "... Crossref	<1%
47	Asian Institute of Technology on 2007-11-09 Submitted works	<1%
48	Benchmarking: An International Journal, Volume 21, Issue 3 (2014-03... Publication	<1%
49	Brisbane Grammar School on 2021-03-25 Submitted works	<1%
50	Encyclopedia of Earth Sciences Series, 2011. Crossref	<1%
51	Osguthorpe, Jeremy. "Characterization and Optimization of Thermal Pr... Publication	<1%
52	School of Business and Management ITB on 2019-09-03 Submitted works	<1%
53	Vietnam National University of Agriculture on 2022-02-14 Submitted works	<1%
54	afni.nimh.nih.gov Internet	<1%
55	opinvisindi.is Internet	<1%
56	anuario.igeo.ufrj.br Internet	<1%

57	degruyter.com Internet	<1%
58	nat-hazards-earth-syst-sci.net Internet	<1%
59	"Advances in Modeling and Interpretation in Near Surface Geophysics",... Crossref	<1%
60	Alexander Mihai Popovici, Sergey Fomel. "Special Global Session and ... Crossref	<1%
61	Becker, Marc R.. "Development of New Methods Involving Strained Het... Publication	<1%
62	Enrico Lunedei, Dario Albarello. "On the seismic noise wavefield in a w... Crossref	<1%
63	Gavaras, George William. "The Automated Environmental Information a... Publication	<1%
64	American Intercontinental University Online on 2011-12-12 Submitted works	<1%
65	Erasmus University Rotterdam Submitted works	<1%
66	Rashed Poormirzaee. "S-wave velocity profiling from refraction microtr... Crossref	<1%
67	Stanko, Markušić, Gazdek, Sanković, Slukan, Ivančić. "Assessment o... Crossref	<1%
68	Tao, Xingtian. "A New Experimental Technique-magnetic Particle Track... Publication	<1%

69	Wei-zhang LIANG, Guo-yan ZHAO, Hao WU, Ying CHEN. "Optimization ... Crossref	<1%
70	Samuel Bignardi, Anthony J. Yezzi, Simone Fiussello, Albert Comelli. "... Crossref	<1%
71	Oleg Khasanov, Zimfir Khasanov, Natalia Khasanova. "The reference m... Crossref	<1%